

Article

Evaluation of the CO₂ Storage Capacity in Sandstone Formations from the Southeast Mesohellenic trough (Greece)

Marina A. Christopoulou¹, Petros Koutsovitis^{1,*}, Nikolaos Kostoglou², Chrysothemis Paraskevopoulou³, Alkiviadis Sideridis¹, Petros Petrounias^{1,4}, Aikaterini Rogkala¹, Sebastian Stock⁵ and Nikolaos Koukouzas^{4,*}

¹ Section of Earth Materials, Department of Geology, University of Patras, 265 04 Patras, Greece; mchrmarina@gmail.com (M.A.C.); a.sideridis@upnet.gr (A.S.); geo.plan@outlook.com (P.P.); krogkala@upatras.gr (A.R.)

² Department of Materials Science, Montanuniversität Leoben, 8700 Leoben, Austria; nikolaos.kostoglou@unileoben.ac.at

³ School of Earth and Environment, University of Leeds, Leeds LS2 9JT, UK; c.paraskevopoulou@leeds.ac.uk

⁴ Centre for Research & Technology Hellas (CERTH), Chemical Process & Energy Resources Institute, 151 25 Athens, Greece

⁵ Institute of Physics, Montanuniversität Leoben, 8700 Leoben, Austria; sebastian.stock@unileoben.ac.at

* Correspondence: pkoutsovitis@upatras.gr (P.K.); koukouzas@certh.gr (N.K.); Tel.: +30-2610-997598 (P.K.); +30-211-1069502 (N.K.)



Citation: Christopoulou, M.A.; Koutsovitis, P.; Kostoglou, N.; Paraskevopoulou, C.; Sideridis, A.; Petrounias, P.; Rogkala, A.; Stock, S.; Koukouzas, N. Evaluation of the CO₂ Storage Capacity in Sandstone Formations from the Southeast Mesohellenic trough (Greece). *Energies* **2022**, *15*, 3491. <https://doi.org/10.3390/en15103491>

Academic Editor: Ben McLellan

Received: 6 April 2022

Accepted: 6 May 2022

Published: 10 May 2022

Publisher's Note: MDPI stays neutral with regard to jurisdictional claims in published maps and institutional affiliations.



Copyright: © 2022 by the authors. Licensee MDPI, Basel, Switzerland. This article is an open access article distributed under the terms and conditions of the Creative Commons Attribution (CC BY) license (<https://creativecommons.org/licenses/by/4.0/>).

Abstract: This study investigates the capability of the Southeast Mesohellenic Trough (SE MHT) sandstone formations to serve as a potential reservoir for CO₂ storage in response to the emerging climate change issues by promoting environmentally friendly mineral sequestration applications. Sandstone samples, for the first time, were evaluated for their petrographic characteristics, mineral chemistry, geochemical properties, as well as their petrophysical and gas adsorption properties through tests. The sandstones were tested and classified into distinct groups. The most promising site to be considered for pilot CO₂ storage testing is the Pentalofos Formation locality since its sandstones display specific mineral phases with the proper modal composition to conceivably react with injected CO₂, leading to the development of newly formed and stable secondary mineral phases. The gas adsorption results are also more encouraging for sandstones from this sedimentary formation. All the measured UCS (uniaxial compressive strength), Ei (bending stiffness), and ν (Poisson's ratio) results are above those dictated by international standards to perform CO₂ storage practices safely. Furthermore, the specified targeted locality from the Pentalofos Formation holds the geological advantage of being overlaid by an impermeable cap-rock formation, making it suitable for deploying CO₂ mineralization practices. The demarcated area could permanently store a calculated amount of $\sim 50 \times 10^5$ tons of CO₂ within the geological reservoir by reacting with the specified mineral phases, as specified through the proposed petrographic PrP index (potential reactive phases).

Keywords: carbon dioxide; mineralization; sandstones; adsorption; storage; capacity

1. Introduction

Climate change has become one of the most significant challenges that humanity is facing, and it poses a threat to a sustainable future. The rapid increase in carbon dioxide emissions in Earth's atmosphere due to excessive burning of fossil fuels and intense industrial activity worldwide has contributed to the observed temperature increase resulting from the greenhouse effect [1–4]. The United Nations Framework Convention on Climate Change (UNFCCC) and the Paris Climate Conference (COP21) call for immediate actions to address global climate change, aiming to vastly reduce CO₂ emissions. Despite the ambition to achieve net-zero CO₂ emissions, CO₂ will continue to be emitted in the atmosphere in rather vast amounts. Therefore, carbon capture and storage (CCS) practices

constitute a vital and sustainable solution to safely capture and permanently store CO₂ and other greenhouse gas emissions (GHG), for which permeable geologic formations are already being considered environmentally safe and economically viable solutions [5,6]. Moreover, throughout lab and field experiments, the potential of CO₂ use for geological carbon storage (GCS) and enhanced oil/gas recovery in shales, as well as the partial replacement of CH₄ with CO₂, has been confirmed [7–9]. In recent years, research has been conducted focusing on determining the most appropriate geological formations as natural reservoirs for CO₂, either for utilization or long-term storage via sequestration, with the formation of new stable mineral phases. Mineral trapping of CO₂ is considered as the safest and most stable geologic CO₂ long-term storage mechanism [10–12].

Geological formations that comprise sandstones have been suggested as suitable reservoirs for capturing and storing CO₂, mainly due to their widespread distribution, high permeability, and preferable mineralogical and geochemical characteristics (i.e., better long-term pH buffer capacity, the reaction of feldspars with CO₂ [13–15], and presence of cap-rocks to retain the buoyant CO₂ within the reservoir rock [16]. Experimental studies that have been conducted upon sandstones, both on a laboratory scale [15–20] and in situ under simulated conditions [21], have shown results that vary from fair to promising, highly depending on the nature of the sandstone examined (e.g., mineral composition and participation percentage, presence of micropores).

The Mesohellenic Trough (MHT) is located in central Greece, constituting a large molassic sedimentary basin of considerable thickness (~5 km). Its main advantages for deploying CCS practices are related to the geological parameters of the hosted formations, i.e., thick sandstone formations often overlaid by relatively impermeable cap-rock formations (mainly pelites). These formations are also considered tectonically stable [16], corresponding to a substantial factor favoring the storage of CO₂. Most studies in the area have focused their efforts on determining the CO₂ amounts that can be potentially stored through numerical computational modeling [22] but without undertaking petrophysical parameters for permanent storage purposes. Additionally, Koukouzas et al. [16] obtained results that were conducted upon sandstone samples from the northeastern part of the MHT with the use of laboratory techniques. To the best of our knowledge, sandstone formations from the southern part of the MHT have not been examined at a laboratory scale to date; thus, it remains unresolved as to whether this specific locality holds a similar potential.

In this scope, the aim of the present study is to provide a mineralogical, petrological, and mechanical characterization of the sandstones cropping out along the southeastern MHT region and to determine the suitability of the geological formations for deploying CO₂ storage practices. Other highlights of this research are to provide storage capacity estimations, mineral sequestration reactions, as well as insights regarding the ability of these formations to act as safe reservoirs.

2. Study Area

The NW–SE-trending Mesohellenic Trough is the largest sedimentary basin (200 km length, 30–40 km width) developed during the last orogenic stage (molasse-type basin) of the Hellenides. The basin was formed between the Mid-Upper Eocene and the Mid-Upper Miocene, at back-arc settings, superimposed on the Olonos–Pindos external and Pelagonian internal geotectonic units [23–26]. This sedimentary basin extends from Albania to the Thessaly region in Greece [26,27] and is located between the Apulian (non-metamorphic) and the Pelagonian (partly metamorphic) microcontinental plates [28].

The Mesohellenic Trough displays a significant lateral extent, and the thickness of the sedimentary formations reach about 4 km in vertical sections. It is also characterized by complicated sedimentary structures and phases [22]. The thicknesses of the deposits, both longitudinally and transversally to the axis of the basin, vary significantly [26]. The sedimentary phases include deltaic conglomerates, alluvial scree, sandstones, and clays belonging to turbiditic sequences and deltaic, floodplain, and sandy shelf sediments.

This study is focused on the southeastern part of the Mesohellenic Trough, which was thoroughly studied and mapped using petrographical criteria, and those results, along with the sampling spots, are presented in the renewed map using the ArcGIS software (Figure 1). The main localities include the Meteora, Mourgani, Oxinia, and Asproklisia. As illustrated in the map, the main lithostratigraphic formations that host the sandstones are, namely, Tsotyli, Pentalofos, and Eptachori. In particular, the stratigraphically lower parts of the Eptachori Formation comprise the clastic Upper Eocene to Lower Oligocene sediments (conglomerates, sandstones). The upper part of the Eptachori Formation is located at the Taliaros Mountain (Grevena–Kastoria; West Macedonia), appearing in the form of local sedimentary phases that mainly include sandstones, marls, and limestones. The sequence’s thickness varies from 1 to 1.50 km. The Pentalofos Formation (Upper Oligocene to Lower Miocene) includes two types of clastic sedimentary rocks separated by marl–sandstone intercalations. Their thickness ranges from 2.3 to 4 km. The Tsotyli Formation (Lower to Middle Miocene) consists of marls accompanied by conglomerates, sandstones, and limestones of variable thickness (0.2 to 1.0 km) [29].

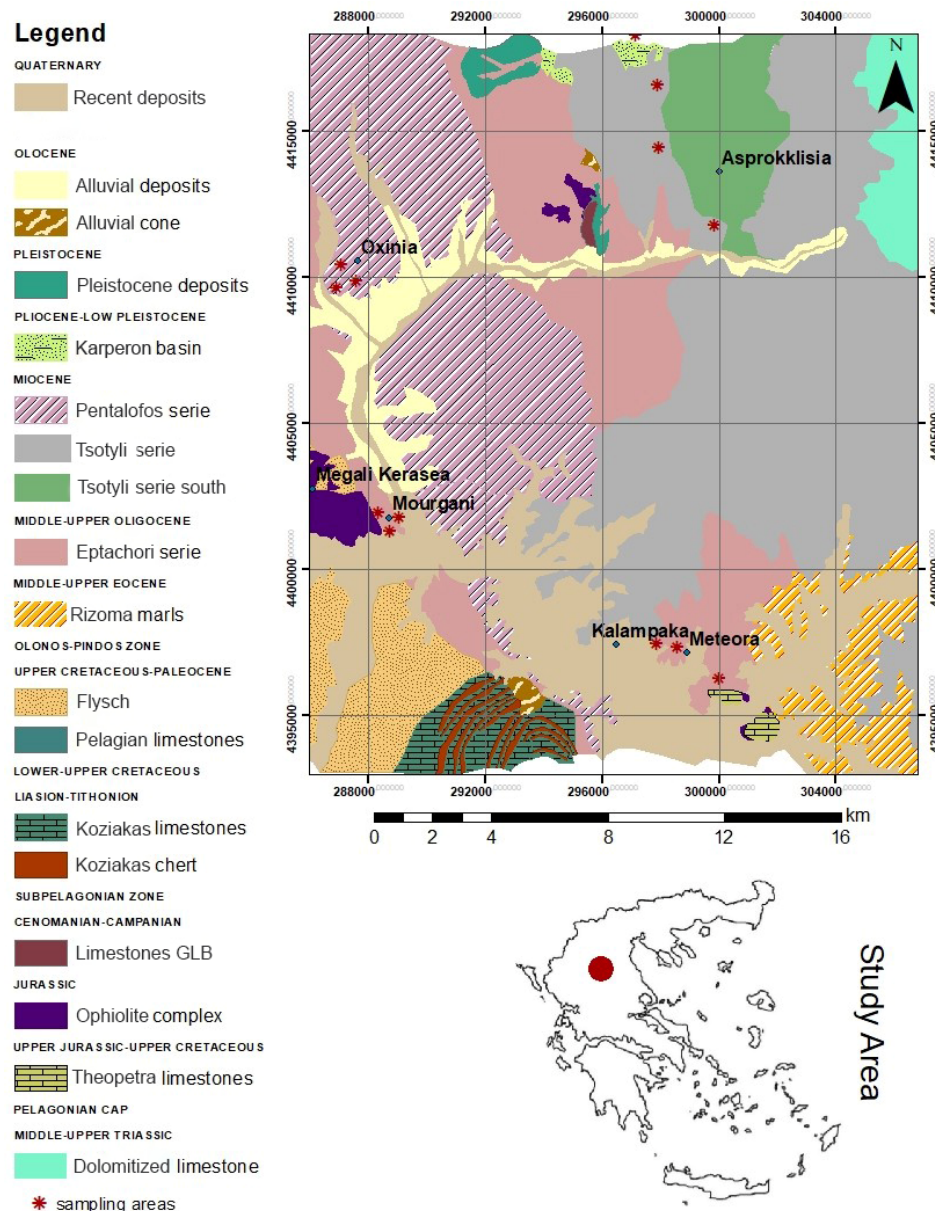


Figure 1. Geological map of the Southeast Mesohellenic Trough (northwest Greece) region (modified after fieldwork mapping).

3. Materials and Methods

3.1. Materials

The study of the SE MHT was conducted upon a range of lithotypes within different geological formations in order for their CO₂ sequestration capacity to be optimally assessed. Thus, after high scrutiny, twelve samples from different types of sandstones (coarse-grained, medium-grained, and fine-grained) were selected from four localities (see Figure 1) as representative of the studied area.

3.2. Methods

The mineralogical and textural characteristics of the studied samples were identified petrographically by examining polished thin sections using of a polarizing petrographic microscope (Leitz Ortholux II POL-BK Ltd., Midland, ON, Canada) following the EN-932-3 [30] standard for the petrographic description of aggregates, emphasizing their mean grain size and grain shape. The bulk mineral composition of the studied samples was also determined through X-ray Diffraction (XRD) facility, using a Bruker D8 advance diffractometer, with Ni-filtered CuK_α radiation. Random powder mounts were prepared by gently pressing the powder into the cavity holder. The scanning angle for bulk mineralogy of specimens covered the 2θ interval 2–70°, with an angular step size of 0.015° and a time step of 0.1 s. The mineral phases were determined using the DIFFRACplus EVA 12[®] software (Bruker-AXS GmbH, Karlsruhe, Germany) based on the ICDD Powder Diffraction File of PDF-2 2006. The semi-quantitative analyses were performed by TOPAS 3.0[®] software (TOPAS MC Inc., Oakland, CA, USA) based on the Rietveld method refinement routine. The routine is based on the calculation of a single mineral-phase pattern according to the crystalline structure of the respective mineral, and the refinement of the pattern using a non-linear least-squares routine. Quantitative errors for each phase were calculated according to the procedures set out in Ref. [31].

Mineral chemistry analyses were performed using a JEOL JSM-6300 SEM (Tokyo, Japan) equipped with energy-dispersive and wavelength dispersive spectrometers and INCA software at the Laboratory of Electron Microscopy and Microanalysis, University of Patras, Greece. Operating conditions were accelerating voltage 25 kV and beam current 3.3 nA, with a 4 μm beam diameter. The total counting time was 60 s and dead-time 40%. Synthetic oxides and natural minerals were utilized as standards for our analyses. Detection limits are ~0.1%, and accuracy better than 5% was obtained. Further examination of the textural features and acquisition of three-dimensional images occurred through an energy-dispersive X-ray spectrometry (EDX) facility at the Department of Chemical Engineering, University of Patras, Greece. Loss on ignition (LOI) in the sample was determined according to the ASTM D7348-13 standard [32]. Whole-rock major and trace element chemistry analyses were derived by using an X-ray Fluorescence (XRF) spectrometer and a sequential spectrometer located at the Laboratory of Electron Microscopy and Microanalysis (University of Patras, Greece). For each sample, 0.8 g of dried ground sample was mixed with 0.2 g of wax (acting as binder) and was pressed to a pellet under 15 tones. Pressed pellets were analyzed with a RIGAKU ZSX PRIMUS II spectrometer (Tokyo, Japan), which is equipped with Rh-anode.

Gas adsorption tests were conducted on all 7 samples in both untreated (whole-rock) and solvent-extracted condition, which were crushed to 80 mesh. The testing was performed at the Montanuniversität Leoben, Austria. Low-pressure N₂ adsorption and desorption isotherms were collected at −196 °C by a Quantachrome Autosorb iQ³ manometric gas sorption analyzer (Boynton Beach, FL, USA). Ultra-pure (99.999%) He and N₂ gases were used for void volume calculations and gas sorption analysis, respectively. Prior to the tests, samples of ~1 g were degassed under high-vacuum (10^{−6} mbar) at 250 °C for 24 h to remove any physisorbed surface species (e.g., moisture, trapped air, etc.). The specific surface areas were calculated by the multi-point Brunauer–Emmet–Teller (BET) method following the pertinent consistency criteria (ISO 9277:2010). The specific pore volumes and average pore sizes were estimated by applying the Barret–Joyner–Halenda (BJH) method

in the N₂ adsorption data (average pore size ranges 0–50 nm). It should be noted that the BJH method is, in principle, not suitable for mesopore analysis in heterogeneous and low-surface area materials, such as the ones presented in this study. However, the BJH-derived data can be used in a qualitative or semi-quantitative manner for a relative comparison between samples showing similar adsorption characteristics. In addition, a low-pressure (0–1 bar) CO₂ adsorption/desorption isotherm was recorded at 0 °C for the sample with the highest surface area using the same gas sorption analyzer coupled with an external temperature controlling device and a circulating bath filled with a mixture of water and antifreezing liquid. The CO₂ gas was also ultra-pure (99.999%).

Baseline unconfined compressive strength (UCS) tests were conducted on seven cylindrical samples of MHT sandstones at the laboratory of the University of Leeds (Rock Mechanics, Engineering Geology and Geotechnical (RMEGG) Laboratories). A modified 2000 kN Walter and Bai servo-controlled rock testing device was utilized. Load was applied in such a way as to maintain a constant radial displacement rate of 0.01 mm/min. Radial displacement was measured using single-strain gauge that was attached to a chain wrapped around the mid height of the specimens, and the axial strain was measured on the sample surface using two-strain gauges at opposite sides of the specimen.

4. Results

4.1. Petrographic Features and Mineral Chemistry

The petrographic study of the examined samples reveals clear and distinctive characteristics amongst the various lithotypes that are directly dependent on the area from which the samples were collected and, therefore, the stratigraphic unit to which they belong.

More specifically, representative sandstones were considered that are derived from the geological Pentalofos Formation that extends throughout the western part of the study area (Figure 1). These are mostly medium- to slightly-coarse-grained sandstones, being moderately sorted, whereas their grains are sub-angular to sub-rounded. The mineralogical composition includes quartz, which forms monocrystalline and polycrystalline grains (mainly undulose—grain contacts generally straight to suture), K-feldspars, plagioclase feldspars, and calcite (Figure 2a). The cement material is mainly siliceous (Figure 2a). The K-feldspars are classified as orthoclase or microcline, whereas the plagioclase feldspars are mostly oligoclase and andesine (Table 1). Clay minerals are also present, represented mostly by halloysite, resulting from the alteration of feldspars (Figure 2b). An increase in the participation of serpentinite fragments within the sandstone matrix constitutes the major characteristic of this group. The main serpentine polymorph is antigorite, with minor amounts of lizardite. The antigorite is characterized by its relatively low Fe and Al amounts (FeO = 3.9–4.9 wt.%, Al₂O₃ = 0.5–2.08 wt.%). Petrographically, they appear in the form of flakes, and, also, XRD patterns confirm their presence (see Section 4.2). Chlorite is present either as diabantite or as ripidolite. Geothermometry calculations based on the thermometer of [33] reveal that these sandstones underwent diagenesis at low-temperature conditions ranging between 89 and 115 °C. The mica phases are represented by muscovite coupled with minor amounts of biotite. The epidote-group minerals comprise clinozoisite and allanite, with highly comparable mineral chemistry with those present in these sandstones. Clinozoisite is characterized by relatively high Al and Ca contents (i.e., Al₂O₃ = 23.2–26.5 wt.% and CaO = 19.7–22.8 wt.%). The allanite grains possess a concentrate CaO ranging from 13.5 to 13.8 wt.%, including considerable amounts of Rare Earth Elements (REE, i.e., Ce₂O₃ = 7.8–8.5 wt.% and La₂O₃ = 3.2–3.8 wt.%).

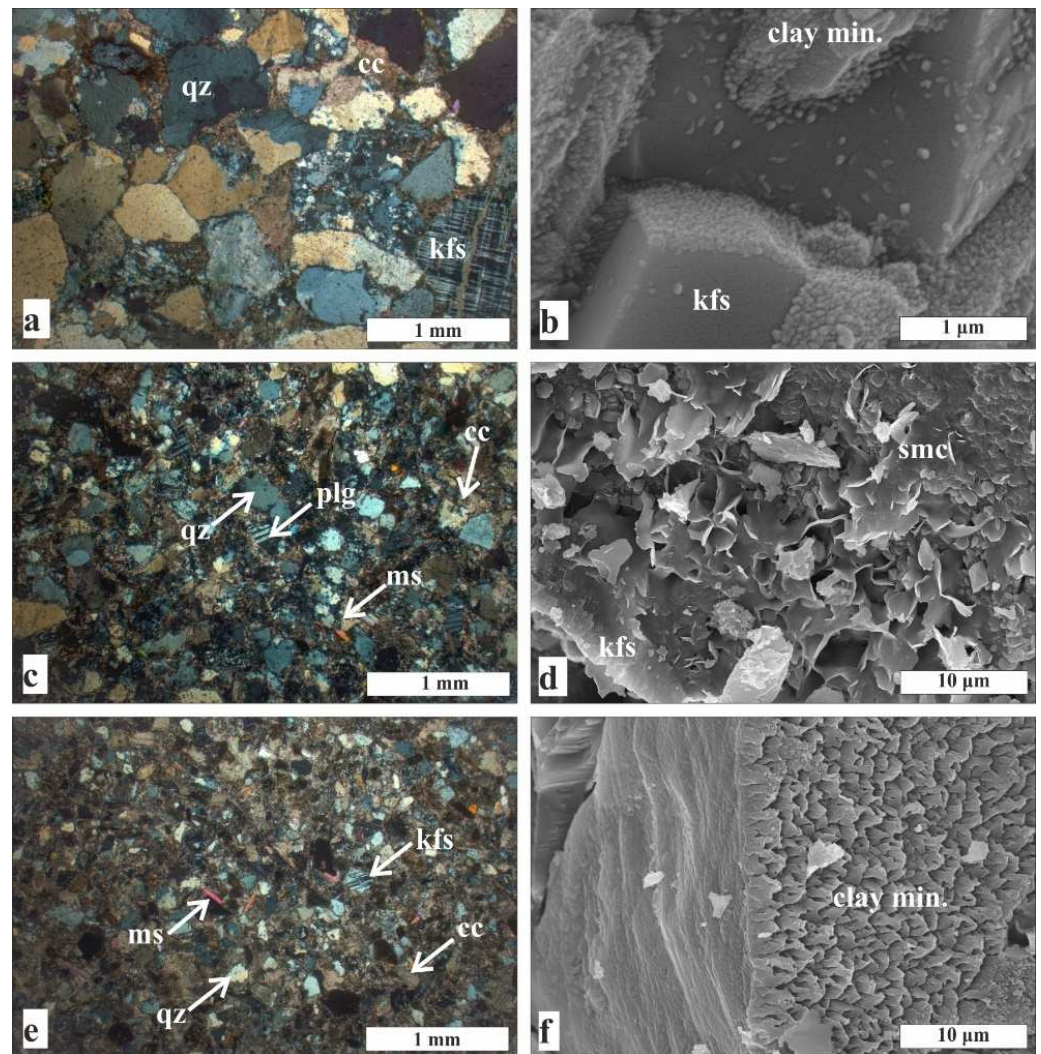


Figure 2. Photomicrographs from optical microscopy showing the textural characteristics of the SE Mesohellenic Trough sandstones and backscattered images (BSI) from SEM: (a) photomicrograph of clastic texture presented in medium-grained sandstone with quartz (Qz), plagioclase (Plg), muscovite (Ms), and calcite (Cc); (b) BSI of smectite formation over K-feldspar; (c) photomicrograph of clastic texture presented in a coarse-grained sandstone with quartz (Qz), K-feldspars (K-Fs), and calcite (Cc); (d) BSI showing alteration of K-feldspar into clays; (e) photomicrograph of clastic texture represented in fine-grained sandstone with quartz (Qz), K-feldspars (K-Fs), muscovite (Ms), and calcite (Cc); (f) BSI showing alteration of K-feldspars and plagioclase into clay minerals.

Table 1. Average and 1σ standard deviation mineral chemistry values of selected sandstone samples from the geological Pentalofos Formation. Abbreviations: Plg: plagioclase, Ab: albite, Olg: oligoclase, Andes: Andesine, Kfs: K-feldspar, Ep: epidote, Srp: serpentine, Bt: biotite, Chl: chlorite, Aln: albanite, Mnz: monazite.

Mineral	Plg (Ab)	Plg (Olg-Andes)	Kfs	Ep	Srp	Bt	Chl	Aln	Mnz
n:	7	5	18	8	6	9	7	3	4
SiO ₂	67.36	62.84	67.04	39.11	45.62	51.33	37.83	40.90	10.74
1σ	0.84	1.37	1.21	1.17	1.10	1.94	2.74	0.95	0.89
TiO ₂	-	-	-	-	-	1.45	-	-	-
1σ	-	-	-	-	-	0.87	-	-	-
Al ₂ O ₃	19.92	23.72	17.44	23.84	1.46	21.54	15.31	22.35	6.18
1σ	1.09	1.64	0.67	1.16	0.74	2.28	1.22	0.91	4.85

Table 1. Cont.

Mineral	Plg (Ab)	Plg (Olg-Andes)	Kfs	Ep	Srp	Bt	Chl	Aln	Mnz
FeO	0.16	0.08	0.16	9.41	6.34	7.41	14.61	12.32	2.07
1 σ	0.09	0.04	0.05	1.48	0.81	2.34	3.18	1.58	1.95
MgO	-	-	-	0.38	33.49	5.27	18.64	-	1.17
1 σ	-	-	-	-	1.63	1.45	3.26	-	-
CaO	1.24	4.32	0.25	24.17	0.59	-	0.79	13.69	3.21
1 σ	0.68	1.30	0.07	1.42	0.12	-	0.20	0.19	3.14
Na ₂ O	10.76	8.62	0.81	-	-	-	-	-	-
1 σ	0.92	0.82	0.62	-	-	-	-	-	-
K ₂ O	0.57	0.29	14.21	-	-	9.57	-	-	-
1 σ	0.23	0.11	0.54	-	-	0.82	-	-	-
P ₂ O ₅	-	-	-	-	-	-	-	-	29.82
1 σ	-	-	-	-	-	-	-	-	4.99
La ₂ O ₃	-	-	-	-	-	-	-	3.85	13.90
1 σ	-	-	-	-	-	-	-	0.43	1.72
Ce ₂ O ₃	-	-	-	-	-	-	-	7.87	29.47
1 σ	-	-	-	-	-	-	-	0.09	2.52
Y ₂ O ₃	-	-	-	-	-	-	-	-	27.08
1 σ	-	-	-	-	-	-	-	-	2.37
Nd ₂ O ₃	-	-	-	-	-	-	-	-	10.48
1 σ	-	-	-	-	-	-	-	-	1.49
Total	99.85	99.87	99.91	96.91	87.19	96.57	87.18	99.05	97.63

The sandstones from the Northern Eptachori Formation (Figure 1) tend to be coarser-grained compared to the sandstones from the Pentalofofos Formation, comprising mostly sub-angular to angular grains (Figure 2b). They are generally moderate- to poor-sorted. The mineralogical composition mainly includes quartz, K-feldspars (orthoclase or microcline), plagioclase, calcite, and, in minor amounts, muscovite, chlorite, and serpentine, as well as lithic fragments (Table 2). Most plagioclase grains are classified as albites, although a few bear slightly higher Ca contents (Table 2). Mica minerals are classified as either biotite or muscovite, with the former being characterized by relatively low Fe-Mg contents (Table 2). According to the classification [34], chlorite is mainly classified as pseudothuringite. Chlorites geothermometry calculations provide important information regarding the conditions of deposition and the diagenesis. In particular, chlorites seem to have been crystallized at relatively elevated temperature conditions that range between 122 and 173 °C (under the calibration of Lanari et al. [33]). Most of the samples investigated comprise serpentine, which is predominantly lizardite, although minor antigorite has been identified. This has been confirmed through petrographic observations and XRD patterns (see Section 4.2). These lizardites are characterized by their relatively elevated Fe contents (i.e., FeO = 7.1–9.8 wt.%). The epidote-group minerals are represented by clinozoisite and allanite. Clinozoisite is characterized by relatively high Al and Ca contents (i.e., Al₂O₃ = 24.1–24.6 wt.% and CaO = 22.1–23.8 wt.%). The allanite grains possess a concentrated CaO ranging from 12.8 to 15.5 wt.%, and they include considerable amounts of REE (i.e., Ce₂O₃ = 8.8–11.3 wt.%). Monazite grains were also encountered, and they are characterized by high REE contents and other incompatible elements (REE + Y + Nd = 27.1–58.3 wt.%). The Northern Eptachori samples present clay cement. Quartz is mostly displayed as undulose monocrystalline and less as polycrystalline grains. The monocrystalline quartz grains (ranging from 0.3 to 0.5 mm) vary from sub-angular to angular, while the polycrystalline counterparts (0.5 to 1 mm) range from sub-angular to sub-rounded. The grain boundaries in most cases are present as sutures. The K-feldspars' grains vary in size (0.4 to 0.7 mm), with angular to subangular shapes, whereas plagioclase is observed in smaller grains (<0.4 mm). In general, the fragments are sub-rounded and sub-angular to angular, and they are mainly comprised of clasts of quartz, feldspars, as well as by rock-fragments of granitic composition, maintaining their granular features.

Table 2. Average and 1 σ standard deviation mineral chemistry values of selected sandstone samples from the Northern Eptachori Formation. Abbreviations: Plg: plagioclase, Ab: albite, Olg: oligoclase, Kfs: K-feldspar, Ep: epidote, Srp: serpentine, Bt: biotite, Chl: chlorite, Aln: alanite.

Mineral	Plg (Ab)	Plg (Olg)	Kfs	Ep	Srp	Bt	Chl	Aln
n:	8	7	11	5	2	6	5	2
SiO ₂	67.55	63.45	66.62	38.52	47.9	52.48	39.24	40.09
1 σ	1.03	1.45	1.28	0.73	0.56	0.73	2.16	0.95
TiO ₂	-	-	-	-	-	1.22	-	-
1 σ	-	-	-	-	-	0.36	-	-
Al ₂ O ₃	19.87	23.38	17.78	24.32	2.03	21.12	14.84	22.35
1 σ	1.31	1.55	1.16	0.44	0.07	2.86	2.33	0.91
FeO	0.19	0.12	0.18	9.69	4.89	7.12	15.76	12.32
1 σ	0.08	0.06	0.11	0.98	0.02	1.83	3.4	1.58
MgO	-	-	-	-	31.58	5.93	16.43	-
1 σ	-	-	-	-	0.67	2.26	2.75	-
CaO	1.11	3.55	0.28	23.76	0.32	-	0.77	13.68
1 σ	0.88	0.80	0.12	0.76	0.05	-	0.42	0.19
Na ₂ O	10.68	9.15	0.83	-	-	-	-	-
1 σ	0.71	0.61	0.42	-	-	-	-	-
K ₂ O	0.46	0.24	14.27	-	-	9.19	-	-
1 σ	0.50	0.22	1.35	-	-	1.13	-	-
La ₂ O ₃	-	-	-	-	-	-	-	3.85
1 σ	-	-	-	-	-	-	-	0.58
Ce ₂ O ₃	-	-	-	-	-	-	-	7.86
1 σ	-	-	-	-	-	-	-	0.09
Total	99.86	99.89	99.96	96.29	86.72	97.06	87.04	100.15

Significant differences were noticed in the sandstones that were sampled from the Southern Eptachori Formation of the study area (Figure 1), comprising relatively fine-grained and well-sorted quartz framework grains that are mainly sub-angular to sub-rounded (Figure 2e), whereas their main characteristic is the development of a fine-grained cement, indicative of this region. The modal composition mostly comprises quartz, K-feldspars, calcite, and mica. Mineral chemistry analyses of the plagioclase grains indicate that they are mainly classified as oligoclase (Table 3). Feldspars are presented in lesser amounts, with the form of orthoclase or microcline. In these sandstones, clay minerals alteration was also noticed (Figure 2f). Muscovite (and, less frequently, biotite) is characterized by relatively low micro-roughness. Chlorite is classified as either as diabantite or ripidolite. The chlorite geothermometry calculations [33] show low temperature diagenetic conditions (i.e., 81–97 °C). Epidote-group minerals comprise clinozoisite Al and Ca contents (i.e., Al₂O₃ = 22.0–22.5 wt.% and CaO = 23.1–23.5 wt.%). Serpentine grains comprise antigorite and lesser lizardite. The antigorite is characterized by its relatively low Fe and Al amounts (i.e., FeO = 4.8–4.9 wt.% and Al₂O₃ = 1.9–2.08 wt.%). Quartz is mostly displayed as undulose. The monocrystalline quartz grains vary from sub-angular to sub-rounded. The grain contacts presented generally as corroded by matrix (Figure 2e). The K-feldspars' grains vary in size (70 to 200 μ m), with angular to subangular shapes, whereas plagioclase is observed in smaller grains (<150 μ m). The cementing material is mainly calcareous (Figure 2e).

Table 3. Average and 1σ standard deviation mineral chemistry values of selected sandstone samples from the Southern Eptachori Formation. Abbreviations: Plg: plagioclase, Ab: albite, Kfs: K-feldspar, Ep: epidote, Srp: serpentine, Bt: biotite, Chl: chlorite.

Mineral	Plg (Ab)	Kfs	Ep	Bt	Chl
n:	5	5	3	4	4
SiO ₂	67.75	66.86	39.67	53.72	39.86
1 σ	1.16	0.63	0.41	2.23	1.47
TiO ₂	-	-	-	0.78	-
1 σ	-	-	-	0.39	-
Al ₂ O ₃	19.65	17.56	23.21	23.72	15.03
1 σ	1.02	0.41	0.33	2.63	0.84
FeO	0.14	0.21	10.41	6.51	16.61
1 σ	0.07	0.09	0.25	2.53	0.36
MgO	-	-	-	4.71	14.82
1 σ	-	-	-	1.61	0.39
CaO	1.18	0.15	23.23	-	0.47
1 σ	0.63	0.06	0.39	-	0.15
Na ₂ O	10.55	0.59	-	-	-
1 σ	0.61	0.32	-	-	-
K ₂ O	0.60	14.53	-	10.32	-
1 σ	0.39	0.33	-	1.07	-
Total	99.87	99.9	96.52	99.76	86.79

4.2. XRD Analyses

The mineralogical-related results reported in Section 4.1 are confirmed by the study of the samples through XRD analysis. In particular, the XRD patterns of random powder mounts from the studied sandstone rocks revealed the mineral assemblages of sandstones derived from the South MHT. Representative XRD patterns from each group of the samples are shown below (Figure 3). In short, the XRD pattern of the OX-3G sample (Pentalofos Formation) displays the mineralogical assemblage quartz (50 vol.%), microcline (20 vol.%), calcite (20 vol.%), and albite (10 vol.%), whereas the sample EPN-2B (Northern Eptachori Formation) consists of quartz (40 vol.%), albite (25 vol.%), calcite (20 vol.%), and muscovite (15 vol.%). On the contrary, the KAL-3B (Southern Eptachori Formation) is composed of quartz (30 vol.%), calcite (30 vol.%), albite (25 vol.%), and microcline (15 vol.%).

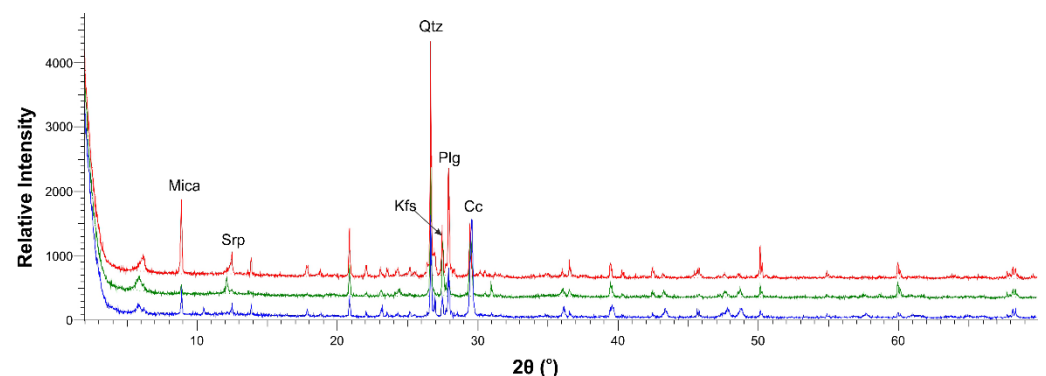


Figure 3. XRD analysis of samples EPN-2B (Northern Eptachori Formation; red-colored), OX-3G (Pentalofos Formation; green-colored), and KAL-3B (Southern Eptachori Formation; blue-colored).

4.3. Clay Fraction

Aiming at the complete mineralogical characterization, the clay fractions of the studied rocks were analyzed since the clay mineral species seem to affect both the CO₂ sequestration capacity and the mechanical characteristics of the studied rocks. Differences were noticed in regard to the clay mineral species participation. The Pentalofos Formation comprises

low concentrations of expanded clay minerals (main component is a mixed layer of illite–smectite, whereas illite dominates) (Figure 4a). An important indication is the appearance of serpentine and chlorite, which predominate. On the contrary, the other two formations are enriched in expanded clay minerals; the Northern Eptachori Formation consists of greater amounts of smectite than illite and chlorite, whereas smectite is mainly noted within the Southern Eptachori Formation. The smectite, under the right conditions, can be greatly expanded, affecting the mechanical properties.

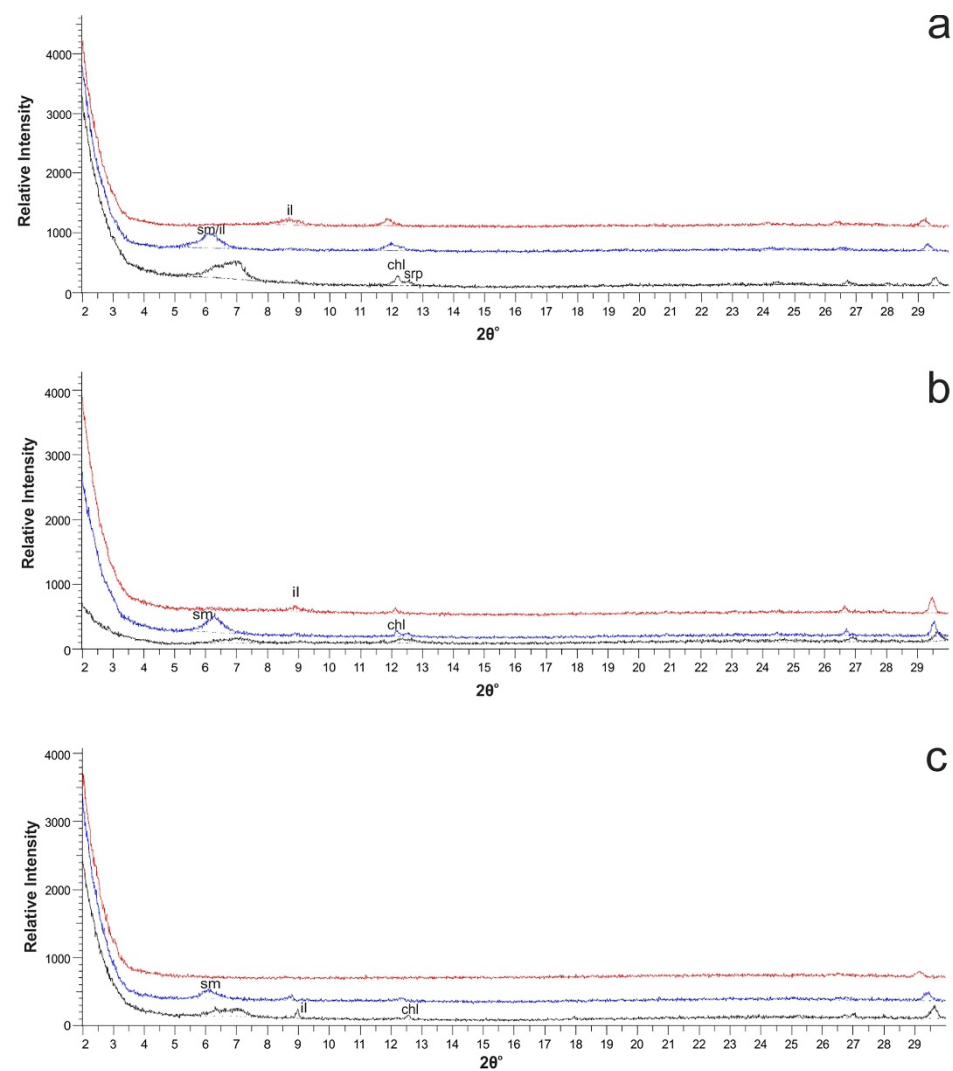


Figure 4. X-ray diffractograms of the clay fraction of representative examined samples: (a) Pentalofos Formation sample, (b) Northern Eptachori Formation sample, (c) Southern Eptachori Formation sample. (Black pattern: air dried; blue pattern: glycolated; red pattern: heated).

4.4. Geochemical Classification

According to the classification diagrams [35,36], the sandstones are distinguished into graywackes and litharenites (Figure 5). Both diagrams denote the same classifications without significant differences. In particular, the sandstones from the Pentalofos Formation are composed of litharenites, which also applies to the sandstones from the Northern Eptachori Formation despite the fact that the latter tend to be coarser grained. On the other hand, the fine-grained sandstones from the Southern Eptachori Formation consist of graywackes and litharenites. The relatively high Ca contents observed in the Southern Eptachori sandstones are attributed to the relatively high abundance of calcite compared to the other two formations, whereas the Ca contents in the other formations with sandstones

mostly reflect the presence of plagioclase, epidote, and allanite. The Mg contents tend to be higher in the Pentalofofos Formation sandstones and the samples from the Northern Eptachori Formation (i.e., MgO up to 5.3 and 8.8 wt.%, respectively) compared to those measured in the Southern Eptachori Formation (i.e., MgO up to 3.6 wt.%) (Table 4).

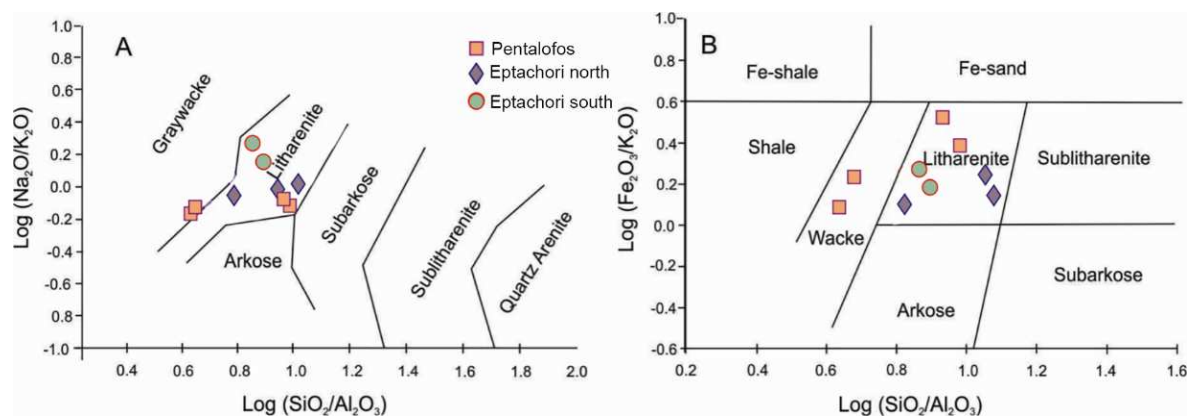


Figure 5. Binary classification plots of (A) $\log(\text{SiO}_2/\text{Al}_2\text{O}_3)$ vs. $\log(\text{Na}_2\text{O}/\text{K}_2\text{O})$ of Pettijohn et al. [35], and (B) $\log(\text{SiO}_2/\text{Al}_2\text{O}_3)$ vs. $\log(\text{Fe}_2\text{O}_3/\text{K}_2\text{O})$ diagram of Herron [36].

Table 4. Whole-rock major (wt.%) and trace element (ppm) compositions of the studied sandstone samples.

Region	Pentalofofos			Northern Eptachori		Southern Eptachori	
Rock Sample	OX-6C	OX-4B	OX-3G	EPN-2B	EPN-5A	KAL-3B	KAL-2C
SiO ₂	59.82	59.46	49.55	68.65	65.98	47.12	48.18
TiO ₂	0.24	0.52	0.26	0.14	0.18	0.24	0.348
Al ₂ O ₃	5.99	12.99	5.22	6.21	5.82	6.81	10.8
FeO *	3.43	3.83	4.46	2.17	1.73	3.72	3.23
MnO	0.18	0.11	0.14	0.05	0.09	0.14	0.15
MgO	5.315	3.63	8.80	3.03	1.92	2.82	1.60
CaO	14.14	7.79	15.57	8.81	12.83	18.53	16.63
Na ₂ O	0.76	2.05	0.74	1.31	1.37	0.91	1.93
K ₂ O	1.08	2.55	0.98	1.40	1.43	1.88	2.81
P ₂ O ₅	0.05	0.07	0.04	0.03	0.04	0.16	0.09
LOI	8.78	5.89	14.12	4.37	8.51	16.39	12.61
Total	99.80	98.90	99.92	96.20	99.94	98.75	98.41
Sc	b.d.l.	6	b.d.l.	4	b.d.l.	b.d.l.	b.d.l.
V	56	85	65	34	40	57	58
Cr	650	280	546	128	162	198	65
Ni	576	154	772	121	141	218	82
Cu	24	25	38	7	9	12	17
Zn	27	51	34	16	21	28	34
Rb	28	105	37	52	41	39	63
Sr	154	139	142	252	215	273	176
Y	14	21	11	11	9	14	20
Zr	75	144	57	76	98	155	119
Nb	b.d.l.	10	20	b.d.l.	b.d.l.	b.d.l.	b.d.l.
Ba	b.d.l.	301	b.d.l.	137	113	b.d.l.	153
Hf	b.d.l.	b.d.l.	b.d.l.	b.d.l.	b.d.l.	44	20
Pb	1	12	b.d.l.	22	14	b.d.l.	4
La	6	21	b.d.l.	12	4	7	13
Ce	3 b.d.l.	37	22	12	11	59	39
Co	23	28	42	19	19	b.d.l.	5
W	b.d.l.	1	b.d.l.	1	1	b.d.l.	1

Ommit symbol *, b.d.l.: below detection limit.

4.5. Gas Adsorption

The notable aspects are the results of the gas adsorption that the studied rocks displayed. Their adsorption capacity correlates with the lithotype distinction and the overall petrographic characteristics. N₂ adsorption/desorption isotherms recorded at $-196\text{ }^{\circ}\text{C}$ for the degassed sandstone samples are presented in Figure 6. All the sandstones from all the studied formations showed a comparable N₂ adsorption/desorption isotherm shape, combining features of type II (macroporous or non-porous) and type IV (mesoporous) isotherms based on the IUPAC classification [37], thus suggesting a similar pore structure. The hysteresis loop formed between the adsorption and desorption curves at $P/P_0 > 0.45$ is usually attributed to capillary condensation in mesopores (i.e., pore widths of 2–50 nm). The hysteresis loop is classified as type H3 according to the IUPAC [37] and is demonstrated by non-rigid aggregates of plate-like particles but also if the pore network consists of macropores that are not completely filled with condensate. The lack of a saturation point at $P/P_0 \sim 1$ describes condensation in macropores (i.e., pore widths $> 50\text{ nm}$) and/or adsorption onto external surfaces. It should be noted that the OX-3G sample from the Pentalofos Formation exhibited the highest adsorbed N₂ volume both at lower ($P/P_0 < 0.1$) and higher ($P/P_0 \sim 1$) relative pressures. This was also confirmed by using the multi-point BET and BJH methods on the N₂ adsorption data to calculate the BET areas and BJH pore volumes, respectively, as displayed in Table 5. The average mesopore diameter values also ranged from 6.6 to 14.9 nm for both fragments and powders (Table 5, Figure S1).

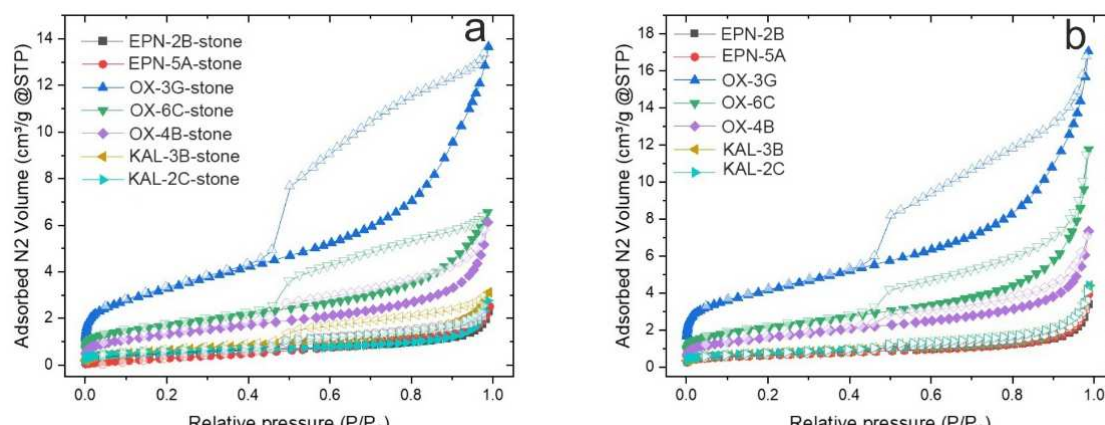


Figure 6. N₂ adsorption (solid symbols) and desorption (open symbols) isotherms recorded at $-196\text{ }^{\circ}\text{C}$ for the degassed sandstones as fragments (a) and fine powders (b).

Table 5. Pore structure properties deduced by N₂ adsorption data recorded at 77 K.

Sandstones	BET Area (m ² /g)		BJH Pore Volume (cm ³ /g)		Average Mesopore Diameter (nm)	
	Fragments	Powders	Fragments	Powders	Fragments	Powders
OX-3G	11.8	14.8	0.018	0.022	7.2	7.1
OX-4B	4.8	5.9	0.008	0.010	7.9	7.7
OX-6C	6.1	7.7	0.008	0.016	6.6	9.4
EPN-2B	1.7	2.4	0.003	0.005	8.4	8.9
EPN-5A	1.5	2.3	0.004	0.005	10.3	10.6
KAL-3B	1.9	2.7	0.004	0.006	8.0	14.9
KAL-2C	2.4	2.5	0.004	0.009	8.8	10.0

In general, the samples belonging to the Pentalofos Formation (i.e., OX-3G, OX-4B, and OX-6C) demonstrate higher surface areas and pore volumes compared to the rest of the formations (Table 5). Pore structure is an important factor that should be considered in studies concerning rock formations as possible CO₂ reservoirs.

After completion of the previous test, the sample with the best performance in the N₂ adsorption-desorption studies (i.e., OX-3G; Pentalofos Formation) was selected for CO₂ sorption analysis at 0 °C; the results are presented in Figure 7.

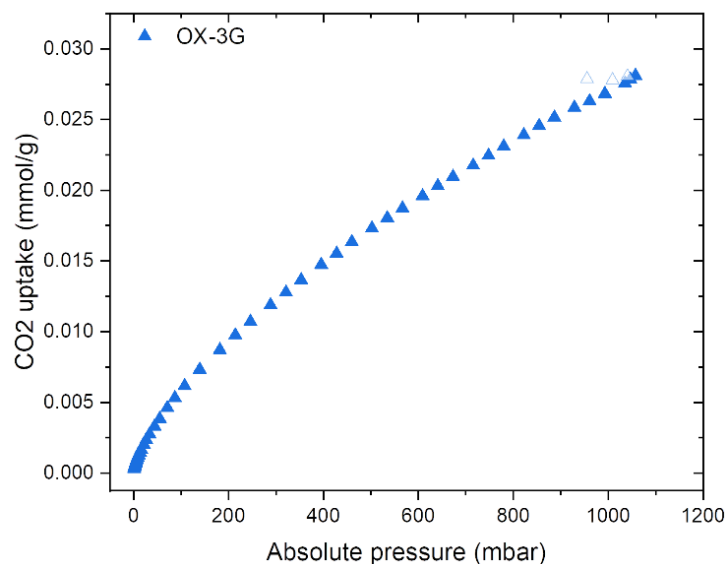


Figure 7. Gas sorption analysis with CO₂ at 0 °C for powder OX-3G sandstone sample from Pentalofos Formation as representative sample. Showing a potential for CO₂ storage within the relevant sandstone sample. Adsorption (solid symbols) and desorption (open symbols).

4.6. Mechanical Tests

Aiming to locate the best rock formation in Greece to act as a successful and safe CO₂ reservoir, we also considered the study of the mechanical properties of the reported sandstones. The test results are presented in Table 6 and Figures 8–11. The physical–mechanical characteristics of the examined samples, as observed in Table 6, show significant variations in their values and are directly dependent on their particular mineral–petrographic characteristics even in the same study areas. For example, the sample OX-3G has a much higher mechanical strength than the sample OX-6C, although they belong to the same formation and have received similar alteration effects; however, the present difference is due to the different percentage of quartz, with the samples showing increased rates of quartz and increased mechanical properties. The correlation between the strength of the rock mass and the percentage of quartz has been reported by Sabatakakis et al. [38]. The mechanical properties of the Pentalofos Formation demonstrate the best results; however, even the rest of the sandstone samples display acceptable mechanical characteristics. In particular, uniaxial static load tests were performed to determine and investigate the behavior of the brittle sandstone rocks under constant (controlled) stress-state conditions. Stress–strain curves for brittle rocks can be used to determine: (1) UCS; (2) E_i ; and (3) ν [39]. The latter is defined as the ratio of the change in lateral width per unit width to change in axial length per unit length caused by the axial stretching or stressing of a material. As illustrated in Figures 8 and 9, it is evident that the samples developed a significant brittle cracking; however, they demonstrated moderate to significant resistance, as shown in the binary strain versus axial stress plots (Figures 10 and 11). In these graphs, three variables are plotted that include the axial stress, the radial strain, and the volumetric strain. The projected plots define curves that yield UCS, E_i , and ν results for each sample, as shown in Table 6. Generally, the UCS results of the sandstones vary from 38 to 272 MPa. More specifically, the sandstone from the Pentalofos Formation displays strength values ranging from 64 to 271 MPa. The Pentalofos Formation displays the highest reported values, meaning that these sandstones are described by high strength, being able to support high uniaxial forces. Concerning the sandstone specimens from the Northern Eptachori Formation, these display

a variety of strength values (88 to 108 MPa), whereas the sandstones specimens from the Southern Eptachori Formation showed high compressive strength values (~38 MPa). The E_i values seem to be generally aligned and consistent with the UCS values. On the other hand, the ν values seem to behave more independently from the above-mentioned parameters due to the fact that, in some cases, the axial stress and radial strain compression may not significantly affect the elasticity, which depends highly upon the mineral constituents and their mode.

Table 6. UCS, E_i , and ν values derived from mechanical tests at the University of Leeds (Rock Mechanics, Engineering Geology and Geotechnical (RMEGG) Laboratories).

Sample	UCS	E_i	ν
	MPa	MPa	
OX-3G	181.85	64,648	0.19
OX-4B	271.89	142,850	0.25
OX-6C	64.66	53,584	0.22
EPN-2B	88.73	34,938	0.22
EPN-5A	108.35	61,923	0.27
KAL-3B	37.7	27,444	0.11
KAL-2C	30.49	34,996	0.15

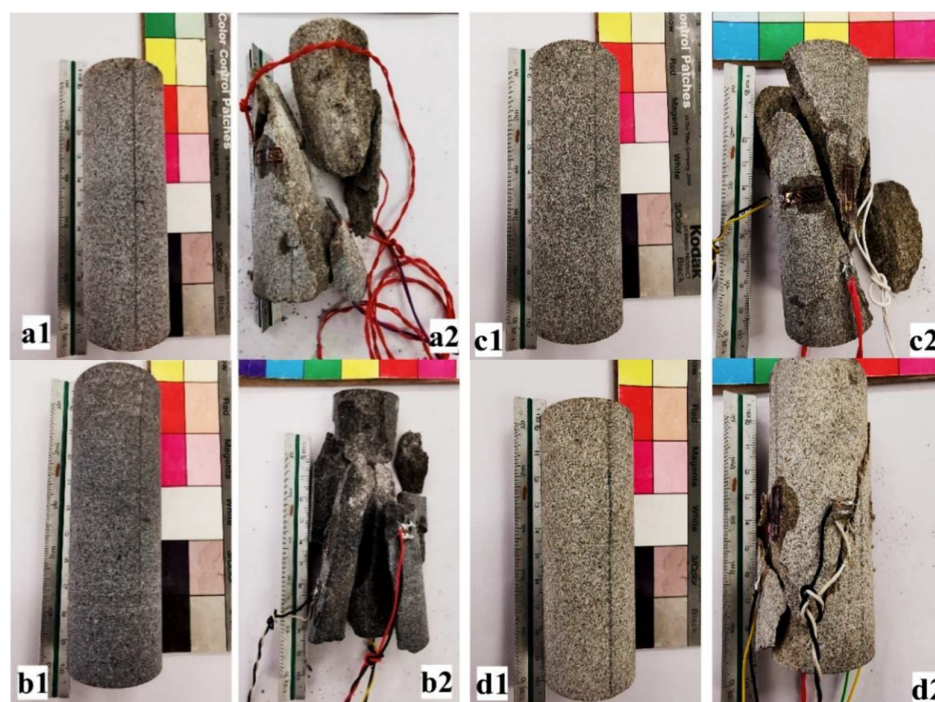


Figure 8. Typical breaks in cylindrical specimens under uniaxial compressive strength before and after the testing of the corresponding samples; (a1,a2) and (b1,b2) are from the Northern Eptachori Formation sandstones (EPN-2B and EPN-5A, respectively), (c1,c2) are from Pentalofos Formation sandstones, and (d1,d2) are from the Southern Eptachori Formation sandstones (samples: OX-3G and KAL-2C, respectively). Note the strain gauge sensors that were employed for the measurements in vertical and horizontal orientations.



Figure 9. Typical breaks in cylindrical specimens under uniaxial compressive strength before and after the testing of the corresponding samples. (a1,a2) (sample OX-6C), (b1,b2) (sample OX-4B) are from Pentalofofos Formation sandstones; (c1,c2) (sample KAL-3B) from Southern Eptachori Formation sandstones. Note the strain gauge sensors that were employed for the measurements in vertical and horizontal orientations.

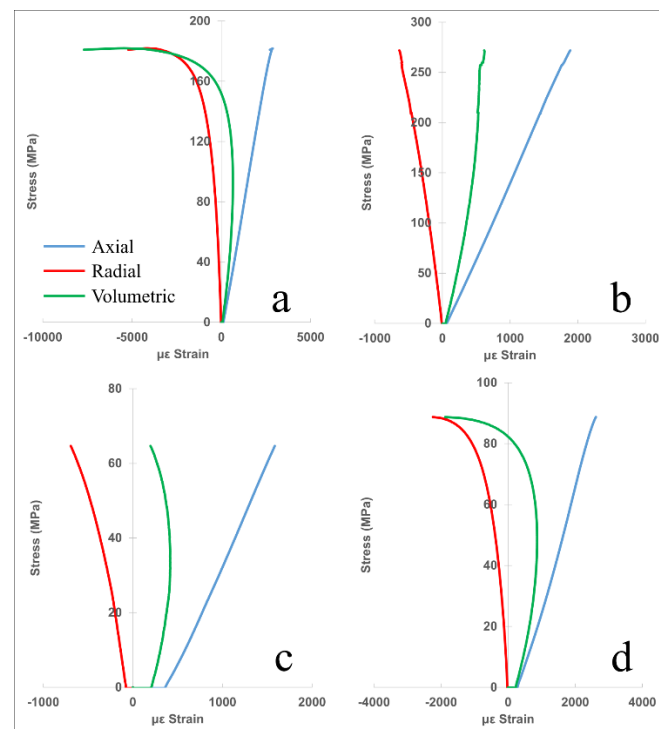


Figure 10. Schematic representations of the stress–strain response and stages of brittle rock fracture process and evolution of the short-term strength of the material to its long-term strength when subjected to a constant stress condition; (a) OX-3G, (b) OX-4B, (c) OX-6C, (d) EPN-2B.

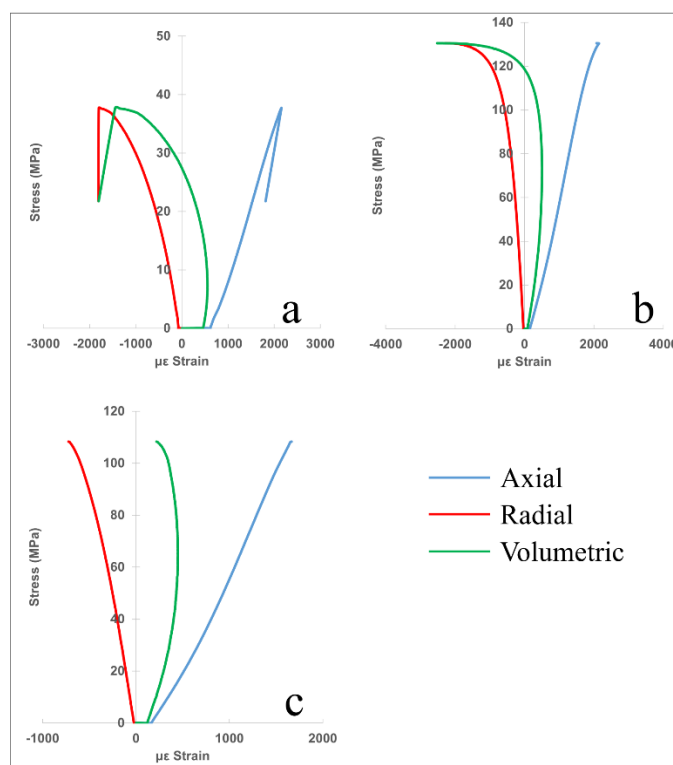


Figure 11. Schematic representations of the stress–strain response and stages of brittle rock fracture process and evolution of the short-term strength of the material to its long-term strength when subjected to a constant stress condition; (a) KAL-2C, (b) KAL-3B, (c) EPN-5A.

5. Discussion

5.1. Suitability of Sandstones for CO₂ Mineralization

A possible means of reducing carbon dioxide (CO₂) emissions to the atmosphere is the injection of CO₂ into structural reservoirs in deep permeable geologic formations [5]. Numerical modeling of geochemical processes is necessary to investigate long-term CO₂ injection in deep geologic formations. The present study was based upon the combination of two important pillars: (a) the detailed mineralogical and petrographical study, and (b) the mechanical properties of the studied rocks in order to test the capability of the MHT-hosted sandstones in Greece to act as potential CO₂ reservoirs.

Through the detailed mineral and petrographical study, the MHT can be divided into three groups based on the distinctions that correspond to local geological formations. In the context of the present study, a normalized approach regarding the modal composition of the studied samples is provided in Table 7, which resulted by deploying the TOPAS software coupled with the petrographic study results.

As shown in Table 7, for the quantification of the mineralogical components, the samples are clearly distinguished into three different groups, corresponding to the three distinct regional geological formations. More specifically, Group 1 consists of the Pentalofos Formation sandstone samples, Group 2 contains the samples of the Northern Eptachori Formation, whereas Group 3 comprises the sandstone samples of the Southern Eptachori Formation. Group 1 demonstrates the least amount of matrix material and quartz content. Moreover, the sandstones of this group are characterized by the presence of noticeable amounts of serpentinite fragments, which are also present in the Group 2 sandstones but in smaller amounts. On the other hand, compared to Group 1, Groups 2 and 3 tend to display higher amounts of quartz, calcite, and matrix material, as well as lower amounts of serpentine, feldspars, and mica. These characteristics are also identified through the geochemical and mineral chemistry analyses listed in Sections 4.1–4.4. It is worth noting that Group 3 consists of smaller amounts of serpentine and chlorite compared to the other

two sandstone groups, whereas the total alkali contents of Groups 1 and 2 remain rather stable without significant differences; this denotes the highly comparable amounts of feldspars present within the sandstone samples of our study.

Table 7. Quantification of modal composition of the representative investigated groups of sandstones. Mineral abbreviations according to Whitney & Evans [40] (Qz: quartz, Kfs: K-feldspar, Pl: plagioclase, Cc: calcite, Dol: dolomite, Srp: serpentine, Chl: chlorite, Ep: epidote).

		Modal Composition										
	Samples	Qz	Kfs	Pl	Cc	Dol	Mica	Srp	Chl	Ep	Cement	P.r.P
Group 1 (Pentalofos)	OX-3G	28.8	20.6	9.9	7.3	2.7	4.4	8.2	4.9	5.1	8.1	1.03
	OX-4B	29.9	22.9	12.2	8.9	2.2	6.3	7.2	3.6	6.0	9.7	1.08
	OX-4C	30.7	19.2	10.7	9.0	2.4	3.8	7.4	3.2	2.8	10.8	0.83
	OX-6C	26.8	22.6	10.9	9.2	2.0	4.2	6.2	3.9	4.1	10.1	1.00
Group 2 (Eptachori north)	EPN-1C	32.8	16.6	12.8	12.3	0.5	2.6	1.4	1.9	2.7	16.4	0.58
	EPN-2B	33.2	13.4	14.6	13.2	0.8	3.1	1.5	2.2	2.8	15.2	0.57
	EPN-4A	31.7	14.8	16.2	14.9	0.5	2.6	0.7	2.8	1.9	13.9	0.59
	EPN-5A	31.6	16.4	15.8	11.6	0.9	3.8	1.5	2.0	1.5	14.9	0.66
Group 3 (Eptachori south)	KAL-1B	31.1	11.7	11.4	22.7	-	1.5	-	2.0	0.8	18.8	0.35
	KAL-2C	34.0	10.9	10.7	19.8	-	2.8	-	2.5	-	19.3	0.33
	KAL-3B	33.2	11.7	12.4	17.2	-	1.6	-	3.0	1.3	19.6	0.39
	KAL-3C	32.9	10.9	11.7	18.4	-	2.4	-	3.5	-	20.2	0.35

Based upon the experimental results of the capacity of the studied rocks to adsorb N₂ gas, as shown in Figure 6, in combination with the pore structure properties (Table 5), it is evident that the initial division into three distinct groups corresponding to the three regional geological formation units is justified. All the studied formations showed a comparable N₂ adsorption/desorption isotherm shape (see Figure 6), combining features of type II (macroporous or non-porous) and type IV (mesoporous) isotherms based on the IUPAC classification [37], thus suggesting a similar pore structure.

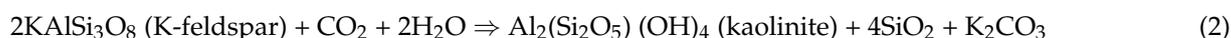
The three groups, apart from being characterized by distinctive mineral assemblages, are also correlated with their specific surface areas and specific pore volumes. The combination of these two factors seems to have an important effect upon the ability of rocks to infuse N₂ aided by adsorption-related processes upon the surfaces of the participating mineral phases, combined with the different types and degrees of porosity. Group 1 generally presents the greatest capacity for N₂ adsorption, followed successively by Group 2 and Group 3 in order of capacity. It should be noted that the OX-3G sample (Group 1—Pentalofos Formation) exhibited the highest adsorbed N₂ volume both at lower ($P/P_0 < 0.1$) and higher ($P/P_0 \sim 1$) relative pressures, which is attributed to its highest surface area and pore volume amongst all the samples, pointing to a formation capable of reserving increased amounts of CO₂ since N₂ exhibits similar kinetic behavior within the rock-building units. This was also confirmed by using the multi-point BET method on the N₂ adsorption data. The calculated BET areas for the degassed sandstones (see Table 5) range between 2 and 12 m²/g and 2 and 15 m²/g for the as-received fragments and the processed powders, respectively, with the OX-3G samples having more than double the value compared to the other samples. A similar trend was observed for the calculated BJH pore volumes, with the highest value (~ 0.02 cm³/g) shown for the OX-3G powder sample. The BET area values presented in this study are comparable to the ones reported for organic-matter-rich shales [41]. The OX-3G sandstone powder sample from the Pentalofos Formation was also investigated using CO₂ adsorption. As shown in Figure 7, the OX-3G sample shows a particular uptake curve with specifically encouraging results regarding the ability of this sandstone to physically retain CO₂ on its porous structure (i.e., a CO₂ uptake of ~ 0.03 mmol/g was recorded at 0 °C and ~ 1 bar). The OX-3G outperforms the rest of the sandstone samples in terms of N₂ and CO₂ uptake. However, its full potential for practical applications can only be deduced by high-pressure (up to 50 bar) CO₂ studies.

This fact indicates that the sandstone rocks of the Pentalofos unit (Group 1) are highly associated with their mineralogical composition and their pore structure properties to successfully achieve CO₂ sequestration (Figure S1). More specifically, there are particular mineral phases that are considered critical in relation to the capacity of a rock to sequester CO₂. These minerals that seem to have a positive effect on sequestration are serpentine, epidote, K-feldspar, plagioclase, and mica-group minerals. On the contrary, quartz, the matrix (given the fact that it is not composed of clay minerals), dolomite, and calcite are reported as inhibitory components. Based on the above and in an effort to combine the presented results with those reported in other research, we propose for the first time a new petrographical index that could represent the capacity of a rock to sequester CO₂:

$$\text{PrP} = (\text{Serp} + \text{Ep} + \text{Kfs} + \text{Pl} + \text{Mica}) / (\text{Qtz} + \text{Cement} + \text{Cc} + \text{Dol}), \quad (1)$$

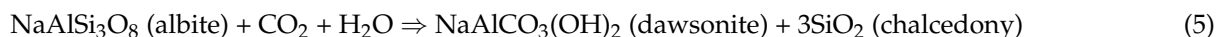
The petrographical findings depending on the results of the PrP index (potential reactive phases) are presented in Table 7, and these demonstrate a clear correlation per studied sandstone group and, therefore, per lithological formation. More specifically, the numerical results of Table 7 and the gas sorption data (Figures 6 and 7) reveal a direct correlation between them, with the apparent trend of the index tending to the unit of “1” as the rock becomes more suitable to retain CO₂ within its structure. The proposed petrographic index of potential binding suitability exclusively for sandstone rocks (PrP) and its correlation depicted in Figures 6 and 7 indicates that mineral phases susceptible to active reaction with injected CO₂ dissolved with water were identified. These minerals include K-feldspars, plagioclase, epidote, chlorite, and serpentine. Some of the sandstones considered in this study contain rather high amounts of the aforementioned minerals, which are occasionally found in other lithological rock types (e.g., basalts and ophiolitic serpentinites) that are considered as suitable for CO₂ mineralization purposes [42–47]. The most common perception is that, in order to achieve CO₂ storage via mineralization, there must be sufficient quantities of Ca-rich plagioclase grains to be partly consumed via alteration reactions so as to successfully lead to the formation of calcite and thus achieve CO₂ mineralization [48]. In recent years, research studies are also considering other mineral phases for reaction with CO₂, forming other mineral phases, such as dolomite, talc, and clay minerals [14,49,50].

Based upon the between-groups distinctions of the sandstones considered in the present study, as well as regarding the mineral chemistry and the determined modal composition, the Group I sandstones incorporate sufficient amounts of K-feldspars that possess the potential of reacting with supercritical CO₂ through the following reactions [14]:

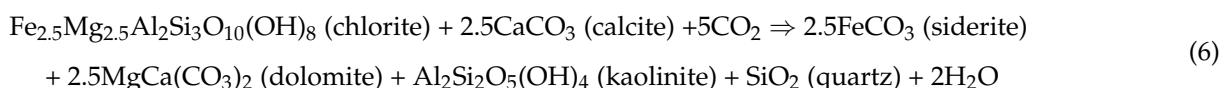


The results from our experimental data (see Section 4.1) suggest that these clay minerals that are standard from Group 1 and the Pentalofos Formation have already been formed in relatively restricted amounts as a natural process of feldspar dissolution; thus, the presence of CO₂ is expected to further facilitate clay mineral mineralization. The Group 3 sandstones that were subjected to more extensive alteration and weathering processes encompass slightly higher amounts of clay minerals, as shown through the clay fraction results. For this reason, despite the fact that plagioclase grains are present in all the sandstone samples considered in our study, they are present in higher amounts in the Group 1 and 2 sandstones. In the Group 1 sandstones, the mineral chemistry of most plagioclase grains is classified as compositionally intermediate, which can serve for the development of both clay minerals as well as calcite. According to Hangx and Spiers [48], it is expected that plagioclase of intermediate or basic composition will form both types of secondary minerals, although it is expected that the clay precipitation will precede that of carbonate. On the other hand, some of the plagioclase minerals in the Group 2 sandstones are albitic, and,

therefore, their alteration is expected to lead to the formation of kaolinite and dawsonite, depending on the rock/water/CO₂ proportions, through the following reactions [14,49]:



The majority of the sandstones considered include chlorite ranging between ~3 and 5 vol.%. Even though these are not regarded as high amounts, they possess the ability to interact with CO₂ and store it as siderite and dolomite [49]. Mineral chemistry analyses of the studied sandstones revealed that most of the chlorite is classified as Mg-rich; hence, it is expected to form through the reaction:



In rocks such as basalts and serpentinites, significant mineralization of water-dissolved CO₂ can be achieved through chemical reactions with the Mg- or Ca-bearing participating mineral phases [44,50–52]. In particular, greenschist facies serpentinites comprise significant amounts of the lizardite serpentine polymorph, which can react with CO₂ to form Mg-rich carbonate minerals [43]:



The PrP index shows that the Group 1 sandstone samples include serpentine in the particular form of lizardite, thus suggesting that CO₂ mineralization can also be achieved through decomposition of this mineral phase. All the sandstone samples that comprise serpentine in their mineral assemblage have been partially replaced by dolomite through relatively restricted alteration processes. Mica minerals comprising both biotite and muscovite are present in amounts in the general range of ~5 to 9 vol.%. Research studies during the past decade have noted the importance of these minerals in sandstones for capturing CO₂, providing further support for the usage of the proposed PrP petrographic index.

In addition, epidote seems to play an important role in the PrP index since epidote has also been considered as a mineral phase that can potentially react with CO₂-charged water injections and since it is a Ca-bearing silicate mineral that can lead to crystallization of relatively high amounts of calcite [53]. The studied sandstones host both Ca-rich and REE-rich epidote-group minerals; these minerals are slightly more frequently included in the Group 1 and 2 sandstones, and partial replacement by calcite has been identified. It is expected that, by injecting CO₂ into the host sandstone rock formations, it will initially result in the decrease in the pH values; the rate depends highly upon the available dissolved CO₂, the alkalinity of the solution, injection period, and reaction conditions [29,54,55]. However, during carbonate precipitation, pH values tend to become neutral [56,57]. According to the findings of Ref. [48], epidote can be partly dissolved under these conditions, releasing the necessary Ca and leading to the crystallization of calcite, starting at temperatures as low as 25 °C, although higher temperatures are expected to further promote epidote dissolution.

Based on the above, it is evident that Group 1 from the Pentalofos Formation possesses the capacity to effectively react and withhold CO₂ via mineralization-related processes, whereas the effect of the mineralogical composition upon the capacity of the sandstone rocks to react with CO₂ is calculated for the first time through the proposed petrographic index, PrP, which ranges between 0.0 and 1.0 depending on the capacity to achieve CO₂ mineralization per lithotype. Despite the fact that the mineralogical assemblages of the Group 1 sandstones display some modal variabilities, the aforementioned reactive mineral phases are, in all cases, present in relatively considerable amounts. Furthermore, the rather restricted presence of typical sandstone amounts of calcite, clay minerals, and quartz suggests that these rocks can be characterized as susceptible to react with CO₂, contrary to the Group 3 sandstones from the Southern Eptachori Formation (Metora site), hindering

the ability for CO₂ storage compared to the sandstone formations represented by the other two groups.

5.2. Recommended CO₂ Storage Site in the Mesohellenic Trough

Geological storage involves injecting CO₂ into rock formations that can absorb and contain it for thousands of years. Rocks well-suited to this are found in sedimentary basins, i.e., areas of subsidence in the Earth crust in which sediments have accumulated over geological periods. Typically, these basins extend for thousands of kilometers. An overarching challenge in CCUS is that the existing sources of CO₂ are very often not located in the vicinity of storage sites. To address this issue, efforts have been undertaken to map the geographical distributions of emission sources and storage formations. Studies [29,58] have examined the MHT for its CO₂ storage potential. Pressure and temperature data, as well as formation depths, were provided in these studies, suggesting an area with high CO₂ storage potential. The pressure gradient appears to have a value of 57 MPa at 2 km with a temperature of 80 °C.

Taking into consideration the petrographic and mineralogical characteristics, as analyzed in the first part of the present discussion and in combination with the satisfactory mechanical characteristics of almost all the rocks of our study, this leads us to propose a well-demarcated area with clear boundaries as a potential reservoir to implement CO₂ storage via mineralization. The mechanical properties of the Pentalofos Formation demonstrate the best results; however, even the rest of the samples demonstrate acceptable mechanical characteristics. The mechanical testing procedures were performed as uniaxial static load tests, and the bending stiffness and Poisson's ratio were performed and calculated to determine and investigate the behavior of the brittle sandstone rocks under constant (controlled) stress-state conditions. All the examined sandstones, and especially the samples of Group 1 and Group 2, show increased mechanical properties as a result of their mineralogical characteristics and the reduced degree of alteration of the formations. A particularly positive feature seems to be the uniform distribution of the secondary minerals within the rock structure as support units appear to be created from the main detrital minerals that tend to function precisely as mechanical support bonds within the sandstone rock structure. A typical example is the continuous alternation of quartz with low-relief phyllosilicate minerals, as described in the petrographic study.

Based on these observations, the Pentalofos and a small part of the Northern Eptachori sandstone formations can be regarded as proper CO₂ reservoirs for permanent storage purposes, especially at localities in which the aforementioned formations hold the geological advantage of being overlaid by the relatively impermeable cap-rock formation of Tsotyli (Figure 12). The example referred to in this paper provides an important potential for storing CO₂ from emitted sources in mainland Greece. These point sources can correspond either to energy production power stations or industrial units. Although the sandy Pentalofos Formation can be considered as a relatively open reservoir, dipping to the NE, the fact that it is sealed by high-stand impermeable shales makes it a suitable formation that can act as a CO₂ storage reservoir.

Based on the above, we can provide preliminary calculations that estimate the CO₂ that could be stored in the frames of a potential pilot project in the studied region of MHT. For this aim, we implement this function:

$$\text{CO}_2 \text{ Storage Capacity} = \Sigma(V \times \phi \times \rho \times \varepsilon) \quad (8)$$

with V symbolizing the sandstone reservoir volume in m³ (under the flysch cap rock); ϕ denoting the effective porosity (%); ρ is the CO₂ specific gravity property (in kg/m³); whereas ε stands for the sCO₂ storage efficiency factor. In the context of the present study, the proposed potential area that meets the necessary conditions to function as a safe CO₂ reservoir has been accurately measured through GIS mapping and was calculated such that it covers an area of 118 km², whereas the depth of the geological reservoir, as delimited from the results of the present study, is defined at about 0.5 km, and, thus, the volume

of the proposed reservoir is 59 km^3 . The cap rock formation that overlies the potential reservoir is about 0.8 km and, therefore, the CO_2 sequestration can be achieved at depths reaching a measure of 1.3 km depth from the surface, allowing for CO_2 injection under supercritical state conditions, which is the most efficient for efficient geological storage. According to van den Meer et al. [59], such storage depths account for a conservative $s\text{CO}_2$ specific gravity property value of 400 kg/m^3 . In addition, based upon the estimations of the authors of Ref. [14] and with reference to the statistical values of USGS (United States Geological Survey) modeling, we can consider the CO_2 storage efficiency factor for sandstones to be 1%. The application of this discount factor is necessary in order to obtain a realistic estimation of the sandstone reservoir storage potential. Taking the aforementioned values into account, as well as additional parameters that include the average sandstone effective porosity values from our studied site (6%), it is assessed that the demarcated area could potentially store an amount of 156×10^5 tons of CO_2 . The actual amount that can in fact react with the selective mineral phases and be stored through mineralization processes can only be roughly estimated because they may react, apart from feldspars, additionally with serpentine, epidote, mica, and chlorite. However, by applying the equation of Jin et al. [14], the amount of CO_2 that is expected to react with the feldspars (K-feldspar and plagioclase) is calculated at 36×10^5 tons of CO_2 . Thus, considering the other mineral phases that have the potential to react with injected CO_2 , we estimate a total amount of $\sim 50 \times 10^5$ tons of CO_2 to be permanently stored within the geological reservoir.

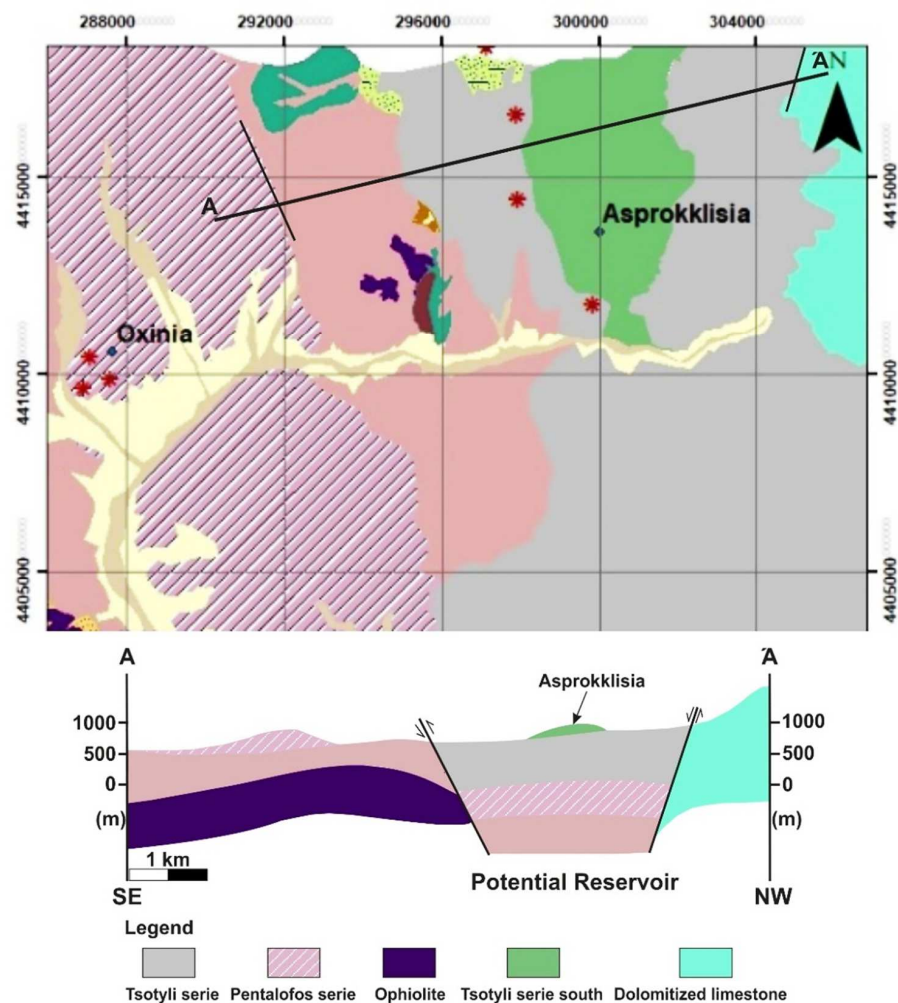


Figure 12. Geological map of the Southeast Mesohellenic Trough (northwest Greece) region and modified model for capacity after fieldwork mapping and experimental study (red star symbols in the map represent sampling areas).

Combining the set of results provided from the present study, it is evident that the study area presents sufficient porosity, permeability, and thickness, as well as sufficient mineralogy, an impermeable flysch cap rock formation, and mechanical strength capable of operating as a safe and large-volume CO₂ reservoir. Porosity and permeability properties that ensure the rock will absorb the CO₂ and significant thickness are critical to containing a substantial volume; these are features enable to perform high rates of CO₂ injection without pressure build-up.

6. Conclusions

In this study, sandstones of various petrographic characteristics derived from the Southeast Mesohellenic Trough were examined for the first time to classify their suitability for potential pilot applications of CO₂ storage in response to the emerging climate change issues by promoting environmentally friendly mineral sequestration applications. In this context, three sandstone groups have been identified, corresponding to the geological formations of Pentalofos (Group I), Northern Eptachori (Group II), and Southern Eptachori (Group III). These groups have been distinguished mainly based upon their petrographic features, mineral chemistry, whole-rock geochemistry, gas adsorption capacity, as well as mechanical testing. The research findings led to the following concluding remarks:

- The petrographic characteristics of the Group I sandstones reveal that they have a better potential for CO₂ storage due to the fact that they contain K-feldspars, plagioclase, epidote, serpentine, chlorite, and mica in relatively significant amounts; these are expected to react with CO₂ and develop newly formed calcite, dolomite, and clay minerals. The latter mineral phases are commonly found in natural soils and, therefore, pose no harm to the environment.
- The proposed petrographic index, PrP, reveals the sandstones that incorporate relatively small amounts of mineral phases and that are susceptible to actively react with CO₂.
- The gas adsorption results seem to be more encouraging for the Group I and II sandstones, coinciding with those that displayed optimal BET analyses results, pore volume values, and mineral modal compositions that are reactive to CO₂ phases.
- The results of the mechanical strength testing of UCS, E_i, and ν revealed that these values highly depend upon the participating mineral phases but also on other parameters, such as their porosity values, as well as their textural features and participation of matrix material. The mechanical results are sufficiently in agreement with international standards to safely perform CO₂ storage practices.
- The most promising site to be considered for pilot CO₂ storage testing from the Southeast Mesohellenic Trough is that located in the Pentalofos Formation since it additionally holds the geological advantage of being overlaid by an impermeable cap-rock formation.
- The demarcated area could permanently store a calculated amount of $\sim 50 \times 10^5$ tons of CO₂ within the geological reservoir by reacting with the specified mineral phases.

Supplementary Materials: The following supporting information can be downloaded at: <https://www.mdpi.com/article/10.3390/en15103491/s1>.

Author Contributions: Conceptualization, M.A.C. and P.K.; methodology, P.K., N.K. (Nikolaos Kostoglou), C.P., A.S., A.R. and P.P.; software, M.A.C., P.K., A.S., P.K. and A.R.; investigation, M.A.C., P.K., N.K. (Nikolaos Kostoglou), P.P., N.K. (Nikolaos Koukouzas), C.P., and A.S.; resources, M.A.C., P.K., A.R. and A.S.; data curation, M.A.C., P.K., A.R., N.K. (Nikolaos Kostoglou) and S.S.; writing—original draft preparation, M.A.C., P.K., P.P. and A.R., writing—review and editing, M.A.C., P.K., P.P., A.R., N.K. (Nikolaos Kostoglou), C.P., A.S. and S.S.; visualization, M.A.C., P.K., A.R., N.K. (Nikolaos Koukouzas) and P.P.; supervision, M.A.C. and P.K. All authors have read and agreed to the published version of the manuscript.

Funding: This research received no external funding.

Institutional Review Board Statement: Not applicable.

Informed Consent Statement: Not applicable.

Data Availability Statement: Not applicable.

Acknowledgments: We kindly thank A. Govatsi of the Laboratory of Electron Microscopy and Microanalysis, University of Patras for his assistance with the microanalyses and SEM micrographs. Many thanks are given to Quentin Fisher for his support for the laboratory testing (University of Leeds). We also thank M. Kalpogiannaki for her assistance in the construction of the geological map. N.K. and S.S. would like to thank Christian Mitterer and Oskar Paris from the Montanuniversität Leoben for providing resources and access to experimental equipment. The Editor and Reviewers are also thanked for their constructive comments and observations.

Conflicts of Interest: The authors declare no conflict of interest.

References

- Bachu, S. Sequestration of CO₂ in geological media: Criteria and approach for site selection in response to climate change. *Energy Convers. Manag.* **2000**, *41*, 953–970. [\[CrossRef\]](#)
- IPCC. *Special Report on CO₂ Capture and Storage*; Cambridge University Press: Cambridge, UK; New York, NY, USA, 2005.
- Li, Q.; Liu, G.; Liu, X.; Li, X. Application of a Health, Safety, and Environmental Screening and Ranking Framework to the Shenhua CCS Project. *Int. J. Greenh. Gas Control* **2013**, *17*, 504–514. [\[CrossRef\]](#)
- Yang, S.; Yu, Q. Experimental investigation on the movability of water in shale nanopores: A case study of Carboniferous shale from the Qaidam Basin, China. *Water Resour. Res.* **2020**, *56*, e2019WR026973. [\[CrossRef\]](#)
- Holloway, S. An overview of the underground disposal of carbon dioxide. *Energy Convers. Manag.* **1997**, *38*, S193–S198. [\[CrossRef\]](#)
- Juanes, R.; Spiteri, E.J.; Orr, F.M.; Blunt, M.J. Impact of relative permeability hysteresis on geological CO₂ storage. *Water Resour. Res.* **2006**, *42*, 395–397. [\[CrossRef\]](#)
- Tolmachev, O.; Urunov, A.; Muminova, S.; Dvoichenkova, G.; Davydov, I. Review of unconventional hydrocarbon resources: Production technologies and opportunities for development. *Min. Miner. Dep.* **2020**, *14*, 113–121. [\[CrossRef\]](#)
- Chen, L.; Zhao, M.; Li, X.; Liu, Y. Impact research of CH₄ replacement with CO₂ in hydrous coal under high pressure injection. *Min. Miner. Dep.* **2022**, *16*, 121–126. [\[CrossRef\]](#)
- Jia, B.; Chen, Z.; Xian, C. Investigations of CO₂ storage capacity and flow behavior in shale formation. *J. Petrol. Sci. Eng.* **2022**, *208*, 109659. [\[CrossRef\]](#)
- Munz, I.A.; Brandvoll, Ø.; Haug, T.A.; Iden, K.; Smeets, R.; Kihle, J.; Johansen, H. Mechanisms and rates of plagioclase carbonation reactions. *Geochim. Cosmochim. Acta* **2012**, *77*, 27–51. [\[CrossRef\]](#)
- Ghacham, A.B.; Cecchi, E.; Pasquier, L.C.; Blais, J.F.; Mercier, C. CO₂ sequestration using waste concrete and anorthosite tailings by direct mineral carbonation in gas–solid–liquid and gas–solid routes. *J. Environ. Manag.* **2015**, *163*, 70–77. [\[CrossRef\]](#)
- Yang, L.; Xu, T.; Feng, G.; Liu, K.; Tian, H.; Peng, B.; Wang, C. CO₂-induced geochemical reactions in heterogeneous sandstone and potential conditions causing the tight cementation. *Appl. Geochem.* **2017**, *80*, 14–23. [\[CrossRef\]](#)
- Wilson, M.; Monea, M. IEA GHG Weyburn CO₂ monitoring and storage project: Summary report 2000–2001. In Proceedings of the 7th International Conference Greenhouse Gas Control Technology (GHGT-7), Vancouver, BC, Canada, 5–9 September 2005.
- Jin, C.; Liu, L.; Yiman, L.; Zeng, R. Capacity assessment of CO₂ storage in deep saline aquifers by mineral trapping and the implications for Songliao Basin, Northeast China. *Energy Sci. Eng.* **2017**, *5*, 81–89. [\[CrossRef\]](#)
- Wang, Y.; Zan, N.; Cao, X.; Cao, Y.; Yuan, G.; Gluyas, J.G.; Lin, M. Geologic CO₂ storage in arkosic sandstones with CaCl₂-rich formation water. *Chem. Geol.* **2020**, *558*, 119867.
- Koukoulas, N.; Kypridou, Z.; Purser, G.; Rochelle, C.A.; Vasilatos, C.; Tsoukalas, N. Assessment of the impact of CO₂ storage in sandstone formations by experimental studies and geochemical modeling: The case of the Mesohellenic Trough, NW Greece. *Int. J. Greenh. Gas Control* **2018**, *71*, 116–132. [\[CrossRef\]](#)
- Alemu, B.L.; Aagaard, P.; Munz, I.A.; Skurtveit, E. Caprock interaction with CO₂: A laboratory study of reactivity of shale with supercritical CO₂ and brine. *Appl. Geochem.* **2011**, *26*, 1975–1989. [\[CrossRef\]](#)
- Huq, F.; Blum, P.; Marks, M.A.W.; Nowak, M.; Haderlein, S.B.; Grathwohl, P. Chemical changes in fluid composition due to CO₂ injection in the Altmark gas field: Preliminary results from batch experiments. *Environ. Earth Sci.* **2012**, *67*, 385–394. [\[CrossRef\]](#)
- Garcia-Rios, M.; Luquot, L.; Soler, J.; Cama, J. Laboratory-Scale Interaction between CO₂-Rich Brine and Reservoir Rocks (Limestone and Sandstone). *Procedia Earth Planet. Sci.* **2013**, *7*, 109–112. [\[CrossRef\]](#)
- Ni, H.; Boon, M.; Garing, C.; Benson, S.M. Predicting CO₂ residual trapping ability based on experimental petrophysical properties for different sandstone types. *Int. J. Greenh. Gas Control* **2019**, *86*, 158–176. [\[CrossRef\]](#)
- Wigand, M.; Carey, J.W.; Schütt, H.; Spangenberg, E.; Erzinger, J. Geochemical effects of CO₂ sequestration in sandstones under simulated in situ conditions of deep saline aquifers. *Appl. Geochem.* **2008**, *23*, 2735–2745. [\[CrossRef\]](#)
- Tasianas, A.; Koukoulas, N. CO₂ Storage Capacity Estimate in the Lithology of the Mesohellenic Trough, Greece. *Energy Procedia* **2016**, *86*, 334–341. [\[CrossRef\]](#)

23. Brunn, J.H. Contribution à l'étude géologique du Pinde septentrional et d'une partie de la Macédoine occidentale. *Ann. Géol.* **1956**, *8*, 346–358.
24. Aubouin, J. Contribution à l'étude géologique de la Grèce septentrionale: Le confins de l'Épire et de la Thessalie. *Ann. Géol.* **1959**, *10*, 525.
25. Papanikolaou, D.; Lekkas, E.; Mariolakos, E.; Mirkou, R. Contribution on the geodynamic evolution of the Mesohellenic trough. *Bull. Geol. Soc. Greece* **1988**, *20*, 17–36.
26. Vamvaka, A. Geometry of Deformation and Kinematic Analysis in Mesohellenic Trough. Ph.D. Thesis, Aristotle University of Thessaloniki, Department of Geology, Thessaloniki, Greece, 2009.
27. Rassios, A.; Moores, E. Heterogeneous mantle complex, crustal processes, and obduction kinematics in a unified Pindos-Vourinos ophiolitic slab (northern Greece). *Geol. Soc. Lond.* **2006**, *260*, 237–266. [[CrossRef](#)]
28. Kiliyas, A.D.; Vamvaka, A.; Falalakis, G.; Sfeikos, A.; Papadimitriou, E.; Gkarlaouni, C.H.; Karakostas, B. The Mesohellenic Trough and the Paleogene Thrace Basin on the Rhodope Massif, their Structural Evolution and Geotectonic Significance in the Hellenides. *J. Geol. Geosci.* **2015**, *4*, 1–17.
29. Koukouzias, N.; Krassakis, P.; Koutsovitis, P.; Karkalis, C. An integrated approach to the coal deposits in the Mesohellenic Trough, Greece. *Bull. Geol. Soc. Greece* **2019**, *54*, 34–59. [[CrossRef](#)]
30. EN 932; Part 3: Procedure and Terminology for Simplified Petrographic Description. European Standard: Warsaw, Poland, 1996.
31. Bish, D.L.; Post, J.E. Quantitative mineralogical analysis using the Rietveld full pattern fitting method. *Am. Mineral.* **1993**, *78*, 932–940.
32. ASTM D 7348; Standard Test Methods for Loss on Ignition (LOI) of Solid Combustion, Residues. ASTM International: West Conshohocken, PA, USA, 2011.
33. Lanari, P.; Wagner, T.; Vidal, O. A thermodynamic model for di-trioctahedral chlorite from experimental and natural data in the system MgO–FeO–Al₂O₃–SiO₂–H₂O: Applications to P–T sections and geothermometry. *Contrib. Mineral. Petrol.* **2014**, *167*, 968. [[CrossRef](#)]
34. Hey, M.H. A review on the chlorites. *Mineral. Mag.* **1954**, *30*, 277–298.
35. Pettijohn, D.E. Ordered and preferential initiation of ribosomal RNA synthesis in vitro. *Nat. New Biol.* **1972**, *235*, 204–206. [[CrossRef](#)]
36. Herron, M.M. Geochemical classification of terrigenous sands and shales from core or log data. *J. Sediment. Res.* **1988**, *58*, 820–829.
37. Thommes, M.; Kaneko, K.; Neimark, A.V.; Olivier, J.P.; Rodriguez-Reinoso, F.; Rouquerol, J.; Sing, K.S.W. Physisorption of gases, with special reference to the evaluation of surface area and pore size distribution (IUPAC Technical Report). *Pure Appl. Chem.* **2015**, *87*, 1051–1069. [[CrossRef](#)]
38. Sabatakakis, N.; Tsiambaos, G.; Ktena, S.; Bouboukas, S. The effect of microstructure on m_i strength parameter variation of common rock types. *Bull. Eng. Geol. Environ.* **2018**, *77*, 1673–1688. [[CrossRef](#)]
39. Paraskevopoulou, C.; Perras, M.; Diederichs, M.; Amann, F.; Löw, S.; Lam, T.; Jensen, M. The three stages of stress relaxation—Observations for the time-dependent behaviour of brittle rocks based on laboratory testing. *Eng. Geol.* **2017**, *216*, 56–75. [[CrossRef](#)]
40. Whitney, D.L.; Evans, B.W. Abbreviations for names of rock-forming minerals. *Am. Mineral.* **2010**, *95*, 185–187. [[CrossRef](#)]
41. Zhang, P.; Misch, D.; Hu, F.; Kostoglou, N.; Sachsenhofer, R.F.; Liu, Z.; Meng, Q.; Bechtel, A. Porosity evolution in organic matter-rich shales (Qingshankou Fm.; Songliao Basin, NE China): Implications for shale oil retention. *Mar. Petrol. Geol.* **2021**, *130*, 105139. [[CrossRef](#)]
42. Matter, J.M.; Kelemen, P.B. Permanent storage of carbon dioxide in geological reservoirs by mineral carbonation. *Nat. Geosci.* **2009**, *2*, 837–841. [[CrossRef](#)]
43. Brown, G.E.; Bird, D.K.; Kendelewicz, T.; Maher, K.; Mao, W.; Johnson, N.; Rosenbauer, R.J.; García Del Real, P. Geological Sequestration of CO₂: Mechanisms and Kinetics of CO₂ Reactions with Mafic and Ultramafic Rock Formations. In *Annual Report to the Global Climate and Energy Project*; Stanford University: Stanford, CA, USA, 2009.
44. Dichicco, M.C.; Laurita, S.; Paternoster, M.; Rizzo, G.; Sinisi, R.; Mongelli, G. Serpentinite Carbonation for CO₂ Sequestration in the Southern Apennines: Preliminary Study. *Energy Procedia* **2015**, *76*, 477–486. [[CrossRef](#)]
45. McGrail, B.P.; Schaef, H.T.; Spane, F.A.; Cliff, J.B.; Qafoku, O.; Horner, J.A.; Thompson, C.J.; Owen, A.T.; Sullivan, C.E. Field validation of supercritical CO₂ reactivity with basalts. *Environ. Sci. Technol. Lett.* **2017**, *4*, 6–10. [[CrossRef](#)]
46. Koukouzias, N.; Koutsovitis, P.; Tyrologou, P.; Karkalis, C.; Arvanitis, A. Potential for Mineral Carbonation of CO₂ in Pleistocene Basaltic Rocks in Volos Region (Central Greece). *Minerals* **2019**, *9*, 627. [[CrossRef](#)]
47. Iglauer, S.; Pentland, C.H.; Busch, A. CO₂ wettability of seal and reservoir rocks and the implications for carbon geo-sequestration. *Water Resour. Res.* **2015**, *51*, 729–774. [[CrossRef](#)]
48. Hangx, S.J.; Spiers, C.J. Reaction of plagioclase feldspars with CO₂ under hydrothermal conditions. *Chem. Geol.* **2009**, *265*, 88–98. [[CrossRef](#)]
49. Gaus, I. Role and impact of CO₂-rock interactions during CO₂ storage in sedimentary rocks. *Int. J. Greenh. Gas Control* **2010**, *4*, 73–89. [[CrossRef](#)]
50. Kampman, N.; Bickle, M.; Wigley, M.; Dubacq, B. Fluid flow and CO₂-fluid-mineral interactions during CO₂-storage in sedimentary basins. *Chem. Geol.* **2014**, *369*, 22–50. [[CrossRef](#)]

51. Aradóttir, E.S.P.; Sonnenthal, E.L.; Björnsson, G.; Jónsson, H. Multidimensional reactive transport modeling of CO₂ mineral sequestration in basalts at the Hellisheidi geothermal field, Iceland. *Int. J. Greenh. Gas Control* **2012**, *9*, 24–40. [[CrossRef](#)]
52. Snæbjörnsdóttir, S.Ó.; Gislason, S.R.; Galeczka, I.M.; Oelkers, E.H. Reaction path modelling of in-situ mineralisation of CO₂ at the CarbFix site at Hellisheidi, SW-Iceland. *Geochim. Cosmochim. Acta* **2018**, *220*, 348–366. [[CrossRef](#)]
53. Marieni, C.; Voigt, M.J.; Oelkers, E.H. Experimental study of epidote dissolution rates from pH 2 to 11 and temperatures from 25 to 200 °C. *Geochim. Cosmochim. Acta* **2021**, *294*, 70–88. [[CrossRef](#)]
54. Snæbjörnsdóttir, S.Ó.; Wiese, F.; Fridriksson, T.; Ármannsson, H.; Einarsson, G.M.; Gislason, S.R. CO₂ storage potential of basaltic rocks in Iceland and the oceanic ridges. *Energy Procedia* **2014**, *63*, 4585–4600. [[CrossRef](#)]
55. Kelemen, P.B.; McQueen, N.; Wilcox, J.; Renforth, P.; Dipple, G.; Vankeuren, A.P. Engineered carbon mineralization in ultramafic rocks for CO₂ removal from air: Review and new insights. *Chem. Geol.* **2020**, *550*, 119628. [[CrossRef](#)]
56. Park, A.H.A.; Fan, L.S. CO₂ mineral sequestration: Physically activated dissolution of serpentine and pH swing process. *Chem. Eng. Sci.* **2004**, *59*, 5241–5247. [[CrossRef](#)]
57. Pokrovsky, O.S.; Golubev, S.V.; Schott, J. Dissolution kinetics of calcite, dolomite and magnesite at 25 °C and 0 to 50 atm pCO₂. *Chem. Geol.* **2005**, *217*, 239–255. [[CrossRef](#)]
58. Arvanitis, A.; Koutsovitis, P.; Koukouzas, N.; Tyrologou, P.; Karapanos, D.; Karkalis, C.; Pomonis, P. Potential Sites for Underground Energy and CO₂ Storage in Greece: A Geological and Petrological Approach. *Energies* **2020**, *13*, 2707. [[CrossRef](#)]
59. Meer, L.G.H.; Hofstee, C.; Orlic, B. The fluid flow consequences of CO₂ migration from 1000 to 600 metres upon passing the critical conditions of CO₂. *Energy Procedia* **2009**, *1*, 3213–3220. [[CrossRef](#)]